


PSFC/JA-01-25

Double Transport Barrier Plasmas in Alcator C-Mod

View metadata, citation and similar papers at core.ac.uk

brought to you by  C
provided by DSpace

C.L. Fiore, R.S. Granetz, M.J. Greenwald, A.L. Hubbard,
J.W. Hughes, I.H. Hutchinson, J.H. Irby, Y. Lin, D. Mossessian,
M. Porkolab, G. Schilling², J.A. Snipes, S.M. Wolfe

October 2001

Plasma Science and Fusion Center
Massachusetts Institute of Technology
Cambridge, MA 02139 USA

¹Present address: General Atomics, San Diego, CA.

²Princeton Plasma Physics Laboratory, Princeton, NJ.

This work was supported by the U.S. Department of Energy, Cooperative Grant No. DE-FC02-99ER54512. Reproduction, translation, publication, use and disposal, in whole or in part, by or for the United States government is permitted.

Submitted for publication to *Nuclear Fusion*.

Double Transport Barrier Plasmas in Alcator C-Mod

J. E. Rice, P. T. Bonoli, E. S. Marmor, S. J. Wukitch, R. L. Boivin[‡], C. L. Fiore,
R. S. Granetz, M. J. Greenwald, A. E. Hubbard, J. W. Hughes, I. H. Hutchinson, J. H. Irby,
Y. Lin, D. Mossessian, M. Porkolab, G. Schilling[†], J. A. Snipes and S. M. Wolfe
Plasma Science and Fusion Center, MIT, Cambridge, MA 02139-4307

[‡]present address: *General Atomics, San Diego, CA*

[†]*Princeton Plasma Physics Laboratory, Princeton, NJ*

Abstract

Double transport barrier plasmas comprised of an edge enhanced D_α (EDA) H-mode pedestal and an internal transport barrier (ITB) have been observed in Alcator C-Mod. The ITB can be routinely produced in ICRF heated plasmas by locating the wave resonance off-axis near $|r/a| \sim 0.5$, provided the target plasma average density is above $\sim 1.4 \times 10^{20}/\text{m}^3$, and can develop spontaneously in some Ohmic H-mode discharges. The formation of the barrier appears in conjunction with a decrease or reversal in the central (impurity) toroidal rotation velocity. The ITB foot is located near $r/a = 0.5$, regardless of how the barrier was produced. The ITBs can persist for ~ 15 energy confinement times (τ_E), but exhibit a continuous increase of the central electron density, up to values near $1 \times 10^{21}/\text{m}^3$ (in the absence of an internal particle source), followed by collapse of the barrier. This barrier is also evident in the ion temperature profiles, and a significant drop of the core thermal conductivity, χ_{eff} , when the barrier forms is confirmed by modeling. Application of additional on-axis ICRF heating arrests the density and impurity peaking, which occurs along with an increase (co-current) in the core rotation velocity. Steady state double barrier plasmas have been maintained for $10 \tau_E$ or longer, with $n/n_{\text{GW}} \sim 0.75$ and with a bootstrap fraction of 0.13 near the ITB foot. The trigger mechanism for the ITB formation is presently not understood.

1. Introduction

Plasmas with internal transport barriers (ITBs) provide an attractive advanced tokamak operational scenario through their enhanced energy confinement and driven bootstrap current. Formation of the ITBs is believed to occur when the $\mathbf{E}\times\mathbf{B}$ shearing rate (proportional to the rotation velocity gradient) exceeds the maximum growth rate for ion temperature gradient driven microturbulence, whence the ion thermal conductivity drops, resulting in improved energy confinement [1]. Most tokamak ITBs are produced with neutral beam injection [2-7], applied during the plasma current rise phase, which leads to $q_0 > 1$ and a non-monotonic q profile; the foot of the ITB is often located near the minimum q value. ITBs have also been produced with $q_0 \sim 1$ in ASDEX Upgrade [5]. In DIII-D, off-axis counter-current beam injection [4] has been used to extend the $\mathbf{E}\times\mathbf{B}$ shearing rate to larger minor radius and thus to broaden the pressure profile for more favorable MHD stability. Quiescent, double transport barrier plasmas have also been produced [6]. Progress toward steady state ITB operation utilizing off-axis lower hybrid current drive in conjunction with neutral beam injection and a variety of feedback control schemes has been demonstrated in JT-60U [3]. Transient optimized shear plasmas with an L-mode edge have been obtained in JET using ICRF power in addition to neutral beams [2]. There is also evidence for a power threshold for ITB formation in JET; the threshold decreases at lower toroidal magnetic field [2].

The connection between ITB formation and plasma rotation in neutral beam heated plasmas is obscured by the inherent momentum input and particle sources. Observations of ITBs in discharges heated solely by ICRF waves or in purely Ohmic H-mode plasmas remove these ambiguities. ITBs have been produced in Alcator C-Mod plasmas [8,9] without neutral beam injection and the main results [8] are summarized here: double transport barrier plasmas consisting of an edge EDA [10] H-mode pedestal and a core ITB, the foot of which is located near $r/a \sim 0.5$, have been obtained with off-axis ICRF (80 MHz) heating ($B_T(0) \leq 4.5$ T). The concomitance of the ITB formation with the slowing of the central toroidal

rotation velocity and the change in sign of the inferred E_r suggests a role of $\mathbf{E} \times \mathbf{B}$ shearing stabilization of the turbulence dominating the core particle and energy transport. The similar ITB characteristics which develop spontaneously in some Ohmic H-mode discharges [8,9] imply that some mechanism other than counter-current rotation [11] driven by ICRF waves or fast particle orbit shifts is dominant in triggering the ITB. In both off-axis ICRF induced and Ohmic H-mode ITBs, the core electron density peaks (up to $10^{21}/\text{m}^3$) continuously in time with no internal particle source. The barriers persist for as long as $15 \tau_E$, then collapse; although $Z_{\text{eff}} < 2$ and the total radiated power fraction is below 50%, excessive core radiation may be a problem. There are sawtooth oscillations throughout most of the ITB period, with the inversion radius ($r/a \sim 0.2$) well inside of the barrier foot; this implies that $q_0 < 1$, and since these barriers form during the plasma current flat top, the q profile is monotonic, confirmed by EFIT [12] calculations.

In this paper several issues will be addressed: thresholds for ITB development, ITB formation with the ICRF resonance on the low field side, and manifestation of the barrier for heat and impurity transport, in addition to steady state ITB control. In Section 2 the experimental setup is reviewed. ITB formation, control and characteristics are described in Section 3, followed by a presentation of modeling and a general discussion in Section 4.

2. Experimental Setup

The observations presented here were obtained from the Alcator C-Mod [13] tokamak, a compact (major radius $R = 0.67$ m, typical minor radius of 0.21 m, and elongation $\kappa \leq 1.8$), high field device ($2.6 \leq B_T \leq 8.0$ T) in the lower single null configuration, which has operated with plasma currents between 0.23 and 1.5 MA and electron densities between 0.2 and $10 \times 10^{20}/\text{m}^3$. Central electron and ion temperatures are typically in the range from 1 to 5 keV, with the electron temperature measured by ECE and Thomson scattering and with the ion temperature

measured by neutron emission and x-ray spectroscopy. Up to 4 MW of ICRF power at 80 MHz [14] are available, and the power is coupled to the plasma by 2 two-strap antennas, each with $0 - \pi$ phasing; the cases described here are with H minority heating in deuterium plasmas. On-axis heating occurs for these antennas at a toroidal magnetic field of 5.3 T. An additional 4 MW of ICRF power are available from a variable frequency (40-80 MHz), variable phase four-strap antenna [15]; for the cases described here, this antenna was operated with $0 - \pi - 0 - \pi$ phasing at a frequency of 70 MHz, which provides on-axis heating for $B_T = 4.6$ T.

For central toroidal rotation measurements, x-ray spectra were recorded with a spatially fixed von Hamos type crystal x-ray spectrometer [16], the line of sight of which is tangent to the plasma axis, pointing in the counter current direction during normal current operation. Central rotation velocities have been determined from the Doppler shifts of the Ar^{17+} Ly_α doublet [17]. Ion temperature profiles and off-axis rotation velocities were determined from the forbidden line, z, in Ar^{16+} , observed with a five chord, spatially (vertically) scannable x-ray spectrometer array [18], with a slight toroidal view. Spectra are typically collected every 20 ms during plasma discharges, and averaged over the sawtooth oscillations which are normally present. Argon is routinely injected into Alcator C-Mod plasmas through a piezoelectric valve.

Electron density profiles were determined by Thomson scattering and from the visible continuum using a high spatial resolution imaging CCD system [19]. Comparison of these *Bremsstrahlung* profiles with the electron density profiles measured by Thomson scattering, which has only six spatial locations in the core plasma, allows Z_{eff} as a function of radius to be determined. The Z_{eff} profiles were interpolated, and used to convert the *Bremsstrahlung* profiles into full electron density profiles with fine spatial resolution. This correction is proportional to $\sqrt{Z_{\text{eff}}}$ and is typically less than 20%. Soft x-ray brightness profiles were measured with two 38 channel diode arrays [20]. Spatial and temporal resolution for this diagnostic, which records x-rays with $h\nu > 2$ keV, are 2.5 cm and 30 μsec , respectively. Radiated

power profiles were determined from a 16 channel XUV diode array [21] which is sensitive to photons with energies above 1 eV, and which has a spatial resolution of ~ 1.5 cm with 100 μ s time resolution.

3. ITB Formation and Control

The prescription for obtaining ITBs with ICRF heating is to place the ICRF resonance well off the magnetic axis, near $|r/a| = 0.5$. First the EDA H-mode develops, reaching the usual plasma parameters in 100-150 ms, corresponding to a few energy confinement times. Subsequently the ITB appears spontaneously and evolves on a longer (~ 400 ms) time scale, with the (EDA H-mode) edge pedestal intact throughout. An abrupt threshold in magnetic field ($B_T < 4.6$ T, resonance location ≤ -0.5) for obtaining ITBs with 80 MHz ICRF waves at 2.7 MW was found (Ref.[8], Fig. 4) as the field was lowered. Operation at high magnetic field (6.6 T), so that the 80 MHz resonance was on the outboard side, was also found to produce an ITB [22], although in this particular discharge, the core density peaking was not associated with a slowing of the toroidal rotation velocity [23], and there was an H-L back transition which is also known to produce peaked density profiles [9]. For the discharge at 6.05 T in Fig. 4 of Ref.[8], there was no density peaking or drop in rotation velocity; however, the target plasma electron density was lower than for the discharges below 4.5 T. Recently it was found that for ITB formation with off-axis ICRF heating, the average electron density of the target plasma (in Ohmic L-mode) must be above $\sim 1.4 \times 10^{20}/\text{m}^3$, which interestingly is near the threshold for obtaining steady EDA H-mode [24]. This condition is demonstrated in Fig. 1, where the central toroidal rotation velocity (400 ms after initiation of the ICRF pulse, which is enough time for the ITB to be well developed) is shown as a function of the average electron density of the target plasma (before! the ICRF pulse). All plasmas had a toroidal magnetic field of 4.5 T and an ICRF frequency of 80 MHz, at power levels above 1 MW. Those plasmas with a negative rotation velocity had

a well established ITB, while those with a positive velocity did not. Similar to the abrupt magnetic field/resonance location threshold for ITB formation is this abrupt threshold in target plasma density. Another scan of the toroidal magnetic field and resonance location has been performed in a series of similar discharges with an ICRF frequency of 70 MHz and power level of 1.5 MW. The time histories of several plasma parameters of interest for two successive discharges, one at 4.12 T and the other at 3.91 T, are shown in Fig. 2. While the 4.12 T discharge exhibited the normal EDA H-mode behavior, with steady electron density and co-current toroidal rotation velocity, the 3.91 T discharge demonstrated a dramatic reduction in the rotation velocity and increase of the central electron density beginning at 0.85 s, both indicative of ITB formation. This situation is very similar to that shown in Fig. 3 of Ref.[8]. In both cases it was the movement of the ICRF resonance outward (to the high magnetic field side) of $r/a = -0.5$ that precipitated the ITB formation. A corresponding shift of the ICRF resonance outward (to the low magnetic field side) of $r/a = +0.5$ has been found in the present experiments to give rise to an ITB, as shown in Fig. 3. In this case, an increase of the toroidal magnetic field from 5.12 T to 5.41 T caused the rotation to drop, the central density to increase and an ITB to form. The results of the complete toroidal field/resonance location scan are shown in Fig. 4. In the top frame are the rotation velocities evaluated at 450 ms after the initiation of the ICRF pulse and in the bottom frame are shown the ratios of the core to outer ($r/a = 0.7$, outside of the ITB foot) electron densities, also at 450 ms into the ICRF heating. With the ICRF resonance outside of $|r/a| = 0.5$, the plasmas had central peaking of the density and a negative rotation velocity, both signatures of ITBs. This indicates that it is not a threshold in absolute magnitude of B_T that matters, but a threshold in ICRF resonance location. The observation of counter-current toroidal rotation with the ICRF resonance on the low toroidal magnetic field side is in contrast to the predicted co-current torque induced by shifts of trapped energetic ion orbits [11].

The necessary conditions for obtaining these ITBs in Ohmic H-mode plasmas are less clear-cut, but one common feature is the magnetic field below 4.6 T.

However, a similarity of off-axis power deposition does not hold for these Ohmic plasmas. Above 5.4 T, the available Ohmic power is insufficient to obtain H-modes and therefore to produce ITBs.

Having established the conditions for barrier formation in off-axis heated ICRF discharges, a detailed discussion of ITB plasma parameter profiles follows. Shown in Fig. 5 are the time histories of several parameters of interest for a 4.5 T plasma, which had an EDA H-mode edge pedestal and a core ITB generated by off-axis ICRF waves. 2 MW of ICRF power at 80 MHz were delivered for the time interval between 0.7 and 1.5 s, as seen by the green curve in the 4th panel of the figure. This deuterium majority discharge had a hydrogen fraction of 4%. The plasma entered H-mode at 0.76 s, as evidenced by the drop in the D_α signal, and the subsequent rises in the plasma stored energy, electron density, ion temperature and central toroidal rotation velocity [23]. The EDA H-mode was well established when around 0.85 s the rotation velocity began to drop in conjunction with the formation of the ITB, as seen in the continuous rise of the core electron density. The ITB formation may be visualized by examination of the evolution of the electron density profiles for this discharge, as demonstrated in Fig. 6. Individual profiles are shown from every 100 ms, starting at 0.575 s. The two purple chain traces are from the Ohmic L-mode portion of the discharge (at 0.575 and 0.675 s); these profiles are relatively flat. The first dashed green curve represents the density profile at 0.775 s, soon after the L-H transition; at this time there was a well defined H-mode edge pedestal [24], and subsequently the profile filled in toward the center, remaining fairly flat. By 0.875 s the ITB began to develop, apparent in the peaking of the core density and with the foot location near $R = 0.80$ m, or $r/a \sim 0.5$. This corresponds to the time that the core toroidal rotation dropped. For the next 300 ms, the density profiles (shown in dashed green) continued to peak in the core, while the outer half of the profile remained quite constant, maintaining the edge pedestal intact, together with the strong ITB, and in the absence of an internal particle source. While this ITB is very pronounced for particles, with a factor of two increase of the core density over the density outside of the ITB, it is less dramatic for energy

transport. This is probably due to the high electron density and the fact that in these experiments, $T_e=T_i$, allowing the electron thermal conductivity to dominate. Shown in Fig. 7 are ion temperature profiles taken for a series of discharges similar to that shown in Figs. 5 and 6. The large dots at the plasma center represent the core ion temperature deduced from the neutron rate, while the other symbols are from Doppler widths of x-ray transitions [18]. The purple points are from the Ohmic L-mode interval (0.5–0.7 s) and the profile is relatively broad. The solid purple curve is proportional to $[1-(\frac{r}{a})^2]^\alpha$ where α is determined by the ratio of the plasma current to the toroidal magnetic field, $\Gamma(\frac{3}{2}\alpha + 1)/\Gamma(\frac{3}{2}\alpha + 2)=0.2Rq_0/a^2$ (I/B), where a is the minor radius (cm), R is the major radius (cm) and q_0 is the central safety factor [18]. For the Ohmic L-mode portion of these discharges, I/B was 17.3 kA/T yielding $\alpha=0.92$, leading to the solid purple curve, which fits the observed profile quite well. During the transient ITB phase of the discharge of Fig. 5 from 0.8 to 1.2 s, the central ion temperature was constant. The ion temperature profile during this time is shown by the green asterisks in Fig. 7; it is clearly more centrally peaked than the Ohmic profile, suggesting that this ITB is an energy barrier as well. This profile is more centrally peaked than the ion temperature profiles in EDA H-mode plasmas without an ITB. The thin green line in Fig. 7 is proportional to the purple curve, and certainly does not represent the observed profile; the thick green curve, which is considerably more peaked in the core, is a fit to the measured profile. Similar shapes have been observed in the electron temperature profiles, which includes an edge pedestal (not measured for the ions).

In previous experiments it was found that following the formation of the ITB, the core electron density peaked continuously, leading to a collapse of the barrier [8]. In recent experiments it has been discovered that by adding a modest amount of on-axis heating power to an ITB discharge (formed by off-axis heating), the increase of the electron density can be stopped and the barrier can be maintained in steady state [25]. This effect is also demonstrated in Fig. 5; at 1.25 s additional heating power at 70 MHz was injected, reaching 600 kW by 1.35 s, as shown in red in the 4th panel. (The total ICRF power is shown in blue.) Not surprisingly, there was

an increase in the plasma stored energy and the central ion temperature after this time. Of particular interest is the return of the co-current toroidal rotation during this interval, indicating an increase in the core E_r , along with a halt to the electron density increase. This freezing of the density profile is demonstrated in Fig. 6, where three profiles, with a central density of $\sim 5.5 \times 10^{20}/\text{m}^3$ during the 200 ms interval between 1.275 and 1.475 s, are shown in red. This value corresponds to 75% of the density limit for this 0.8 MA discharge. As was apparent from Fig. 5, the central ion temperature increased with the on-axis heating; the complete profile is shown in red in Fig. 7. This profile has the same peaked shape as the one during the rising density ITB phase (green), as evidenced by the red curve, which is proportional to the thick green curve. Besides the arrest of the electron density peaking and the increase in the core ion temperature, there are other beneficial effects from the additional on-axis heating, as is demonstrated in Fig. 8. Between 1.35 and 1.5 s, the ambient level of central soft x-ray emission was held constant. Note that throughout the ITB phase of this discharge, sawtooth oscillations were present, and that the sawtooth inversion radius was near $R = 0.73$ m ($r/a = 0.2$), well inside of the ITB foot location. Similarly, the additional on-axis heating stemmed the increase of the total radiated power, holding it at a tolerable level of about 50% of the total input power. Likewise, Z_{eff} was maintained at a constant value of 1.8 during this time. In Fig. 8 is also shown the ratio of the central electron density to the value at $R=0.83$ m, well outside of the ITB foot, reiterating the arrest of the density peaking.

Although the modest rise in the total radiated power during the transient ITB phase (0.8–1.3 s) shown in Fig. 8 appears benign, examination of the time evolution of the radiated power emissivity profiles reveals an intense increase in the core radiation during this time interval, as shown in Fig. 9. During the Ohmic L-mode (purple chain curves) and the initial EDA H-mode portion of the discharge (0.575–0.775 s), the radiation profile was highest near the plasma edge. Once the ITB formed and the core electron density began to rise, there was an extreme peaking of the radiation profile near the plasma core, with the break point location inside of the electron density ITB foot. After application of the 70 MHz ICRF,

the radiation profile was also held nearly steady, although highly peaked. Similar peaked impurity profiles during the ITB phase are found from an examination of the spectrally resolved argon x-ray emission. Shown in Fig. 10 are brightness profiles of argon x-ray lines between 3.94 and 4.00 Å, which originate from helium-like Ar¹⁶⁺ and nearby lithium-like satellites [26]. During the Ohmic L-mode phase of this series of similar discharges (as in Fig. 7), the brightness profile was relatively flat (purple asterisks) while during the steady ITB phase, the brightness profile was highly peaked (red dots), with over a factor of 20 increase in the core. Similar observations have been made with the (spectrally unresolved) x-ray array [8].

Regarding external control of the ITB plasma parameters, the peak electron density may be regulated by varying the delay time of the on-axis heating power after the initial off-axis ICRF used to create the barrier. Earlier application of the on-axis heating arrests the central electron density at a lower value. This effect is demonstrated in Fig. 11 where the central electron density and ICRF waveforms for two different 4.5 T plasmas are shown. In both cases the ITB was formed by ~ 2 MW of 80 MHz heating power applied between 0.7 and 1.5 s. The difference between the two discharges was the delay time of the additional 500-600 kW of on-axis heating power at 70 MHz. With the shorter delay of 250 ms, the central density was held just above $4 \times 10^{20}/\text{m}^3$ whereas with the longer delay of 550 ms, the central density was arrested at a higher value near $5.5 \times 10^{20}/\text{m}^3$. If the delay is too short, there isn't time for the barrier to form; if the delay is too long, the barrier will collapse due to excessive core radiation.

The characteristics of the ITB plasmas are affected by the power level of the additional on-axis heating used to stabilize the barrier. Shown in Fig. 12 is a comparison of three 4.5 T discharges with similar target parameters, ITBs initiated by 2 MW of 80 MHz ICRF power applied between 0.7 and 1.5 s, and three different power levels of on-axis heating at 70 MHz added between 0.95 and 1.5 s. The discharge shown in black had no additional on-axis heating and demonstrated the usual unregulated ITB development behavior: a drop and reversal (to counter-

current) of the central toroidal rotation velocity and a continuous rise of the core electron and impurity densities, followed by a collapse of the barrier. The discharge shown in red had 530 kW of 70 MHz power which held the barrier steady for 500 ms, nearly 15 energy confinement times. The discharge shown in green had 930 kW of 70 MHz power which regenerated a strong, increasing co-current toroidal rotation velocity and slowly decreasing core electron density, indicating a steadily weakening ITB. This power level at the plasma center is too strong to maintain the ITB in steady state. The electron density profiles for these three discharges, measured at 1.25 s, are shown for comparison in Fig. 13, with the same color code. The discharge with no on-axis heating exhibited the strongest ITB (with the highest density peaking) whereas the discharge with strong central heating displayed an unremarkable density peaking.

For completeness it should be noted that barriers formed at 5.4 T with low field side off-axis heating at 70 MHz have been successfully stabilized with on-axis 80 MHz heating power, demonstrating the flexibility of ICRF ITB control.

4. Modeling and Discussion

As was presented in the previous Section, the electron density, ion temperature and radiated power profiles have been determined for both the evolving (0.8–1.25 s) and steady state (1.35–1.45 s) ITB portions of ICRF heated discharges similar to that shown in Fig. 5. In order to perform the complete energy balance analysis of these ITB plasmas, the ICRF power deposition profiles must first be determined. The energetic hydrogen ion tail production and ICRF power deposition profile were computed using the bounce-averaged Fokker-Planck code FFP [27] coupled to the electromagnetic field solver TORIC [28]. The calculated ICRF power deposition profile from the 80 MHz antennas at the end of the transient ITB phase (1.25 s) for the discharge of Fig. 5 is shown in Fig. 14 by the dashed green curve; it peaks near $r/a = 0.45$ at a value of 7 MW/m^3 . The total integrated power inside of the barrier at this time was about 1 MW. The deposition profile near the end of the two

frequency heating steady state ITB portion of the discharge is shown by the solid red curve in Fig. 14. At this time there were nearly 14 MW/m^3 delivered near $r/a = 0.1$, for an integrated total of about 1.6 MW inside of the barrier. From a comparison with Fig. 9 it can be seen that without core heating, the ITB collapses when $P_{\text{Rad}} > S_{\text{RF}}$, and that with a modest amount of core heating, the core radiation will not exceed the input power.

Using the ICRF power deposition profiles determined in this way, the effective thermal conductivity (χ_{eff}) profile evolution may then be calculated from the observed density and temperature profiles utilizing the TRANSP code [29]. (It is more appropriate to consider χ_{eff} in this case rather than the individual thermal conductivities for ions or electrons since at these high densities, the two temperature profiles are the same within the experimental uncertainties, and small differences would lead to unsubstantiated conclusions about the individual conductivities.) Shown in Fig. 15 are the radial profiles of the calculated χ_{eff} values for three different times during the discharge of Fig. 5, at 0.7 s just before initiation of the ICRF heating, at 1.25 s near the end of the evolving ITB phase and at 1.45 s after the ITB has been stabilized with the 70 MHz ICRF power. During the Ohmic L-mode phase, the χ_{eff} profile was fairly flat, with a value just above $1 \text{ m}^2/\text{s}$. When the ITB was fully developed at 1.25 s, there was a substantial drop (nearly a factor of 10) in χ_{eff} inside the barrier foot, to near neo-classical levels, confirming that this ITB is a true energy barrier. With the application of the on-axis heating power and ITB stabilization, the χ_{eff} profile increased, but was still a factor of three below the L-mode value in the core. It is worth noting that if χ_{eff} were unchanged during the ITB period, one would expect a strong decrease in $T_e(0)$ and $T_i(0)$ as $n_e(0)$ increases, which is not seen.

With the steep pressure gradients associated with the ITB (Figs. 6 and 7), a significant bootstrap current is expected to be driven in the plasma core. This is supported by TRANSP calculations and is shown in Fig. 16. During the steady ITB phase, a current density of nearly 1 MA/m^2 is inferred to peak near $r/a = 0.3$;

a maximum bootstrap fraction of 0.13 occurs at $r/a = 0.45$ at this time.

The behavior of the impurity transport coefficients in ITB plasmas near the barrier foot may be addressed from a comparison of the observed argon x-ray brightness profiles of Fig. 10 with those predicted using the impurity transport code MIST [30], in conjunction with the atomic physics package LINES [31]. Shown in Fig. 10 by the purple chain curve is the calculated brightness profile using the previously determined [32] L-mode transport coefficient profiles, which are reproduced in Fig. 17, also by the purple chain curves. In Ohmic L-mode the impurity diffusion coefficient is highly anomalous while there is no evidence for any inward convection velocity. During the steady ITB phase, a radical modification to the impurity transport coefficients is necessary in order to reproduce the highly peaked argon x-ray brightness profile. Simply using the ITB electron density and temperature profiles, together with the argon density profiles calculated using the L-mode impurity transport coefficients, leads to the red chain curve of Fig. 10, which has the same shape as the L-mode brightness profile and does not represent the observed profile. The solid red curve of Fig. 10, which does an excellent job of matching the data, was generated using the transport coefficients shown in red in Fig. 17. These are very close to the calculated neo-classical impurity transport coefficient profiles shown by the dashed green curves. For these ITB plasmas both the thermal and impurity transport approaches neo-classical levels in the core. It should be noted that using only steady state impurity brightness profiles does not uniquely determine the impurity transport coefficients; modeling of temporally evolving brightness profiles following impurity injection is necessary [32]. Other combinations of diffusion and convection profiles can also match the observed argon x-ray brightness profiles during the ITB phase. Regardless of the actual impurity diffusion coefficient and convection velocity profiles, the deduced impurity density profiles (and x-ray brightness profiles) are highly peaked near the plasma core, more so than the electron density profile. The observations are *consistent* with the impurity transport approaching neo-classical levels in ITB plasmas.

The mechanism for ITB production via off-axis ICRF heating, and for ITB stabilization with on-axis ICRF heating, remains unknown. The association of the ITB formation with changes in the core toroidal rotation velocity, and hence changes in E_r , is well established [8], qualitatively supporting the paradigm of velocity shear suppression of the turbulence dominating energy and particle transport [1]. Unfortunately, without the complete velocity profiles and core turbulence measurements, nothing more definitive can be concluded. The mechanism which generates the co-current core toroidal rotation in the first place is similarly unknown [23]. It is not driven by ICRF waves or through fast particle effects since similar observations have been made in purely Ohmic H-mode plasmas [33,34]. Likewise the ITB formation is probably not an ICRF or fast particle effect either since similar ITB behavior has also been seen in purely Ohmic H-mode plasmas [8,9].

Future experiments will involve more complete rotation and fluctuation profile measurements. The unanswered question of why the barrier foot is located near $r/a = 0.5$ will be addressed by changing the q profile, by operation over a range of plasma currents, although the toroidal magnetic field has been varied in the present experiments. Further means of stabilizing the ITB will be pursued, including toroidal magnetic field ramping and tailoring of the ICRF resonance position.

5. Conclusions

Double transport barrier plasmas have been created in Alcator C-Mod using off-axis ICRF heating with the wave resonance located outside of $|r/a| \sim 0.5$. ITB plasmas have been produced using 70 MHz ICRF waves, with off-axis heating both on the high field side and low field side, with $|r/a| > 0.5$. There is an abrupt density threshold for ITB formation; target plasmas with an average electron density below $1.4 \times 10^{20}/\text{m}^3$ do not develop ITBs. The signature for ITB formation is a decrease and reversal of the central toroidal rotation velocity in conjunction with a steep increase of the electron density profile inside of $|r/a| \sim 0.5$. For these ITB plasmas there is no internal particle or momentum source. The barrier is also evident in

the ion temperature profiles. ITBs have been held in steady state for longer than 10 energy confinement times by means of application of additional on-axis ICRF heating. The additional on-axis heating arrests density and impurity peaking, and also has the benefit of central ion and electron heating. By varying the timing of the on-axis heating following the ITB formation, the central electron density may be held steady for a range of values. Too much central heating degrades the ITB. Modeling of these ITB plasmas suggests a substantial drop (a factor of ~ 10) of the core thermal diffusivity, with impurity transport coefficients approaching neo-classical values. A calculated bootstrap fraction of 0.13 at $r/a = 0.45$ is driven for ITB plasmas with $n/n_{\text{GW}} \sim 0.75$ and with $q_0 \sim 1$. The mechanism for the ITB formation is unknown.

6. Acknowledgements

The authors thank J. Terry for D_α measurements, P. Diamond for useful discussions, D. Lee for assistance with the ICRF experiment and the Alcator C-Mod operations and RF groups for expert running of the tokamak and the ICRF systems. Work supported at MIT by DoE Contract No. DE-FC02-99ER54512.

References

- [1] K. Burrell, Phys. Plasmas **4** (1997) 1499.
- [2] A. Bécoulet et al., Nucl. Fusion **40** (2000) 1113.
- [3] T. Oikawa et al., Nucl. Fusion **40** (2000) 1125.
- [4] V. S. Chan et al., Nucl. Fusion **40** (2000) 1137.
- [5] O. Gruber et al., Nucl. Fusion **40** (2000) 1145.
- [6] C. M. Greenfield et al., Phys. Rev. Lett. **86** (2001) 4544.
- [7] T. J. J. Tala et al., Plasma Phys. Control. Fusion **43** (2001) 507.
- [8] J. E. Rice et al., Nucl. Fusion **41** (2001) 277.
- [9] C. L. Fiore et al., Phys. Plasmas **8** (2001) 2023.
- [10] M. Greenwald et al., Nucl. Fusion **37** (1997) 793.
- [11] F. W. Perkins et al., Phys. Plasmas **8** (2001) 2181.
- [12] L. L. Lao et al., Nucl. Fusion **25** (1985) 1611.
- [13] I. H. Hutchinson et al., Phys. Plasmas **1** (1994) 1511.
- [14] S. N. Golovato, M. Porkolab, Y. Takase et al., in *Proceedings of the 11th Topical Conference on Radio-Frequency Power in Plasmas*, Palm Springs, CA 1995, AIP Conference Proceedings 355 (Editors: Ronald Prater, Vincent S. Chan) American Institute of Physics, Woodbury, New York 1996 p.23
- [15] G. Schilling et al., in *Proceedings of the 14th Topical Conference on Radio-Frequency Power in Plasmas*, Oxnard, CA 2001, American Institute of Physics, Woodbury, New York (to be published)
- [16] E. Källne, J. Källne, E. S. Marmor and J. E. Rice, Phys. Scr. **31** (1985) 551.
- [17] E. S. Marmor et al., Phys. Rev. A **33** (1986) 774.
- [18] J. E. Rice et al., Rev. Sci. Instrum. **66** (1995) 752.
- [19] E. S. Marmor et al., Rev. Sci. Instrum. **72** (2000) 940.
- [20] R. S. Granetz and L. Wang, in *International School of Plasma Physics-9, 1991, Proceedings of Diagnostics for Contemporary Fusion Experiments, Varenna, Italy* Editrice Compositori, Bologna, Italy, p.425.
- [21] R. L. Boivin et al., Rev. Sci. Instrum. **70** (1999) 260.

- [22] S. J. Wukitch et al., in *Plasma Physics and Controlled Nuclear Fusion Research 1998* Proceedings of the 17th International Conference, Yokohama, IAEA-F1-CN-69/CDP/10.
- [23] J. E. Rice et al., Nucl. Fusion **39** (1999) 1175.
- [24] A.E. Hubbard, R.L. Boivin, R.S. Granetz *et al.*, Plasma Phys. Contr. Fusion **40**, 689 (1998).
- [25] P. T. Bonoli et al., in *Proceedings of the 14th Topical Conference on Radio-Frequency Power in Plasmas*, Oxnard, CA 2001, American Institute of Physics, Woodbury, New York (to be published)
- [26] J. E. Rice et al., Phys. Rev. A **35** (1987) 3033.
- [27] G.W. Hammett, “Fast ion studies of ion cyclotron heating in the PLT tokamak”, Ph.D. Dissertation, University Microfilms International No. GAX86-12694, Princeton University (1986).
- [28] M. Brambilla, Nucl. Fusion **38** (1998) 1805.
- [29] R. J. Hawryluk, in *Proceedings of the Course in Physics Close to Thermonuclear Conditions, Varenna, 1979* (Commission of the European Communities, Brussels, 1980), Vol. I, p. 19.
- [30] R.A. Hulse, Nucl. Tech./Fus. **3** (1983) 259.
- [31] M.A.Graf, “Impurity Injection Experiments on the Alcator C-Mod Tokamak”, Ph.D. Dissertation, Massachusetts Institute of Technology (1995)
- [32] J. E. Rice et al., Phys. Plasmas **4** (1997) 1605.
- [33] I. H. Hutchinson et al., Phys. Rev. Lett. **84** (2000) 3330.
- [34] J. E. Rice et al., Phys. Plasmas **7** (2000) 1825.

Figure Captions

Fig. 1 The central toroidal rotation velocity 400 ms after initiation of the ICRF pulse as a function of the average density of the target plasma for 4.5 T, 0.8 MA discharges with 80 MHz waves for power levels greater than 1 MW. The red points, above $1.42 \times 10^{20}/\text{m}^3$, had well established ITBs, while the green points, below the 'threshold', did not.

Fig. 2 Parameter time histories for a 4.12 T discharge (green dashed line) and a 3.91 T discharge (red solid line). Top frame: plasma stored energy and ICRF power. 2nd frame: central ion temperature. 3rd frame: central electron density. Bottom frame: central toroidal rotation velocity.

Fig. 3 Parameter time histories for a 5.12 T discharge (green dashed line) and a 5.41 T discharge (red solid line). Top frame: plasma stored energy and ICRF power. 2nd frame: central ion temperature. 3rd frame: central electron density. Bottom frame: central toroidal rotation velocity.

Fig. 4 The central toroidal rotation velocity (top frame) and core-to-edge electron density ratio (density peaking, bottom frame) as a function of the toroidal magnetic field/ICRF resonance location, evaluated at 450 ms after the initiation of the ICRF pulse, are shown for a series of similar 0.8 MA discharges with 70 MHz waves at 1.5 MW. The discharges shown in red had well established ITBs, while those shown in green did not.

Fig. 5 Parameter time histories for a double barrier plasma. In the top panel is the plasma stored energy, and in the 2nd and 3rd panels are the central electron density and ion temperature, respectively. In the 4th panel is the ICRF power at 80 MHz (green) and 70 MHz (red), with the total shown in blue. D_α emission is shown in the 5th frame and in the bottom panel is the central toroidal impurity rotation velocity. The D_α oscillation at 60 Hz, which began at 1.0 s, is due to up-down

plasma motion of ± 1 cm, because of a vertical position feedback problem.

Fig. 6 Electron density profiles shown every 100 ms, beginning at 0.575 s, for the double transport barrier plasma of Fig. 5. The purple chain curves are from the Ohmic L-mode portion of the discharge, while the dashed green and solid red traces are from the evolving and steady state ITB phases, respectively.

Fig. 7 Ion temperature profiles a series of double transport barrier discharges similar to that shown in Figs. 5 and 6. Central ion temperatures deduced from the neutron flux are shown as large dots at $r=0$. The other symbols represent T_I from x-ray Doppler measurements; purple \times s, green asterisks and red diamonds are from the time intervals between 0.5–0.7 s, 0.8–1.2 s and 1.3–1.4 s, respectively. Typical error bars are shown. The solid purple curve is $930 \text{ eV} [1-(\frac{r}{a})^2]^{0.92}$ and the thin green curve is $1300 \text{ eV} [1-(\frac{r}{a})^2]^{0.92}$. The thick green and red curves are fits to the observed profiles.

Fig. 8 Time histories of the central soft x-ray brightness (top), total radiated power (2nd frame) and Z_{eff} (3rd frame) for the discharge of Fig. 5. In the bottom frame is ratio of the central electron density and that at $R = 0.83 \text{ m}$ ($r/a = 0.7$), outside of the ITB foot.

Fig. 9 Radiated power emissivity profiles shown every 100 ms, beginning at 0.575 s, for the double transport barrier plasma of Fig. 5. The purple chain curves are from the Ohmic L-mode portion of the discharge, while the dashed green and solid red traces are from the evolving and steady state ITB phases, respectively.

Fig. 10 Measured Ar^{16+} and Ar^{15+} x-ray brightness profiles from the Ohmic L-mode phase (purple asterisks) and steady state ITB phase (red dots). MIST simulations are shown by the lines.

Fig. 11 Control of the steady state ITB core electron density by delaying applica-

tion of on-axis heating power. Top frame: central electron density, bottom frame: ICRF waveform, green solid curves: 250 ms delay, red chain curves: 550 ms delay.

Fig. 12 A comparison of plasma parameters for three discharges with differing amounts of on-axis heating power: black curves – 0 MW, red curves – 0.53 MW, green curves – 0.93 MW.

Fig. 13 A comparison of electron density profiles evaluated at 1.25 s for the three discharges of Fig. 12, with the same color coding: black dots – 0 MW, red asterisks – 0.53 MW, green triangles – 0.93 MW.

Fig. 14 Calculated ICRF power deposition profiles at 1.25 s (dashed green) and 1.45 s (solid red), from TORIC.

Fig. 15 Radial profiles of χ_{eff} computed from TRANSP at times 0.7, 1.25 and 1.45 s are shown by the purple chain, dashed green and solid red curves, respectively.

Fig. 16 Radial profiles of the bootstrap current computed from TRANSP at times 0.7, 1.25 and 1.45 s are shown by the purple chain, dashed green and solid red curves, respectively.

Fig. 17 Radial profiles of the impurity diffusion coefficients (top frame) and convection velocities (bottom frame) used in the MIST simulations. Ohmic L-mode (purple chain), steady state ITB (solid red) and neo-classical values for the ITB plasma (green dashed).

